[ur] DIMENSIONS
The Journal of Undergraduate Research in Natural Sciences and Mathematics
Volume 23 | Summer 2022

[ur] DIMENSIONS
The Journal of Undergraduate Research in Natural Sciences and Mathematics
Volume 23 | Summer 2022

## Marks of a CSUF graduate from the College of Natural Sciences and Mathematics

### GRADUATES FROM THE COLLEGE OF NATURAL SCIENCES AND MATHEMATICS:

Understand the basic concepts and principles of science and mathematics.

Are experienced in working collectively and collaborating to solve problems.

Communicate both orally and in writing with clarity, precision, and confidence.

Are adept at using computers to do word processing, prepare spreadsheets and graphs, and use presentation software.

Possess skills in information retrieval using library resources and the internet.

Have extensive laboratory, workshop, and field experience where they utilize the scientific method to ask questions, formulate hypotheses, design and conduct experiments, and analyze data.

Appreciate diverse cultures as a result of working side by side with many people in collaborative efforts in the classroom, laboratory, and on research projects.

Have had the opportunity to work individually with faculty members in conducting research and independent projects, often leading to the generation of original data and contributing to the research knowledge base.

Are capable of working with modern equipment, instrumentation, and techniques.

## DIMENSIONS

DIMENSIONS: The Journal of Undergraduate Research in Natural Sciences and Mathematics is an official publication of California State University, Fullerton. DIMENSIONS is published annually by CSUF, 800 N. State College Blvd., Fullerton, CA 92834. 

### ABOUT THE COVER

The image in the cover was taken by Dr. Merri Lynn Casem and shows a rainbow over Dan Black Hall at CSUF.

## DIMENSIONS Editorial Staff and Thanks


### EDITOR-IN-CHIEF

Melissa Fernandez - Biological Science

### EDITORS

Alisa Hernandez - Biological Science

Melvin Williams - Biological Science

Caitline Batees - Geological Science

Naman Shah - Geological Science

Bianca Cervantes - Mathematics

Cindy Rodas - Mathematics

### ADVISOR

Tatiana Pedroza - Assistant Dean for Student Affairs

### GRAPHIC DESIGN

Alva Duenas - Layout Design

### COLLEGE OF NATURAL SCIENCES & MATHEMATICS

Dr. Marie Johnson - Dean

Dr. Sean E. Walker - Associate Dean

Dr. Merri Lynn Casem - Chair, Department of Biological Science

Dr. Peter de Lijser - Chair, Department of Chemistry and Biochemistry

Dr. Adam Woods - Chair, Department of Geological Sciences

Dr. Alfonso Agnew - Chair, Department of Mathematics

Dr. Ionel Tifrea - Chair, Department of Physics

**Special Thanks To**

The NSM administrative staff for their support, the faculty for advising students and providing them with valuable research opportunities and Tatiana Pedroza for her guidance and oversight.

## Table of Contents


## 7 Biological Science

8 Defining the microbiota's response to and influence on immune defense in *Drosophila* populations
- **Author: Melissa Fernandez**
- **Advisor: Parvin Shahrestani, Ph.D.**

9 Does Size Matter? Surfperch (Family: Embiotocidae) Urogenital Papillae
- **Author: Angelina Guzman**
- **Advisor: Kristy L. Forsgren, Ph.D.**

11 Rat carcass consumption as a pathway of secondary rodenticide exposure for wildlife in natural areas of southern California
- **Author: Gabriela Guzman**
- **Advisor: Paul Stapp, Ph.D.**

20 Whydah you follow Munias around? Pin-Tailed Whydah population growth in Southern California, tracks that of potential brood host, the Scaly-Breasted Munia
- **Author: Alisa Hernandez**
- **Advisor: William J. Hoese, Ph.D.**

21 Influence of the Microbiota on Host Phenotypes in *Drosophila melanogaster*
- **Author: Michaelangelo Marcellana**
- **Advisor: Parvin Shahrestani, Ph.D.**

23 Effects of a non-indigenous bryozoan on the recruitment of the native Olympia Oyster, *Ostrea lurida*
- **Authors: Leeza-Marie Rodriguez and Valerie Goodwin**
- **Advisor: Daniella C. Zacheral, Ph.D.**

## 24 Geological Sciences

25 Exploring the Evidence for Pluton Emplacement Mechanisms in the Jackass Lakes Pluton, California
- **Author: Brandon Jennings Cugini**
- **Advisor: Valbone Memeti, Ph.D.**

26 Using plagioclase geochemistry to examine the degree of magma mixing between the Kuna Crest sheeted complex and lobe magmas during the initiation of magmatism in the Tuolumne Intrusive Complex, California
- **Author: Vincent Mugica**
- **Advisor: Valbone Memeti, Ph.D.**

27 The Volcanic-Plutonic Connection in the Jackass Lakes Pluton
- **Author: Ashleigh Quiroz**
- **Advisor: Valbone Memeti, Ph.D.**

29 Using Charcoal to Reconstruct a Fire History of the Carrizo Plains, CA
- **Author: Dahlia Serrato**
- **Advisor: Dr. Matthew Kirby**

## 30 Mathematics

31 Exploring Classical Guitar Playing Techniques Through Signal Processing
- **Author: Victor H. Sanchez**
- **Advisor: Kristin Kurianski, Ph.D.**

## 43 Authors

# Biological Science

## Defining the microbiota's response to and influence on immune defense in *Drosophila* populations

**Author: Melissa Fernandez**
**Advisor: Parvin Shahrestani**

### ABSTRACT

Studies of longevity, immunity, and gut microbiota have sparked interest in the healthcare field, as the connections among these traits have potential to guide medical treatments. Already, we have shown in the Shahrestani lab that selection for extended longevity is associated with improvement in immune defense and changes in the microbiota. We propose to more directly study the connections among microbiota, longevity, and immunity through experiments in which we manipulate the microbiota of long- and short- lived populations of *Drosophila melanogaster* and test for impacts on host lifespan and immune defense. Specifically, we begin with four types of *D. melanogaster* populations, which differ in their first age of reproduction and in longevity. The generation times for these four types of populations are 10-days (A-type), 14-days (B-type), 28-days (C-type), and 70-days (O-type). Each population type is five-fold replicated. We use a process called dechlorination to remove the outer chorion layer of eggs laid by age-controlled parents from each population. Dechlorination causes the eggs to become sterile, completely free of bacteria. We then introduce controlled bacterial conditions as follows: sterile eggs on conventional diet, sterile eggs on diet supplemented with acetic acid bacteria (known to reduce lifespan), sterile eggs on diet supplemented with lactic acid bacteria (known to improve lifespan), sterile eggs on diets with both acetic acid and lactic acid bacteria, sterile eggs on sterile diet, and conventional eggs on conventional diets. The specific acetic acid and lactic acid species are selected based on what we have already shown to be the predominant species in the *D. melanogaster* microbiota. We next closely monitor developing flies to determine the impact of host genotype and microbial condition on development rate, which is closely correlated with lifespan. Five days post eclosion, we homogenize and plate *D. melanogaster* from each group to determine host genetic control of the microbiota. Since flies from all four population types receive the same treatments, if the bacteria grow to different abundances and compositions in the different fly genotypes, that would suggest that host genotype has influence on the success of the microbiota. For conventional flies on conventional diets, we expect to replicate our prior results, which is that development time in increasing order should show A-types, B-types, C-types, and then O-types, and we expect results for bacterial abundance to be in the exact opposite order. But we expect that experimentally manipulating the microbial conditions will show genotype-by-environment interactions. Lastly, we will assess the immune defense against the entomopathogen *Providencia rettgeri* through survival and microbial abundance assays to determine the extent to which the relationship between immunity and longevity is mediated by the gut microbiota.

## Does Size Matter? Surfperch (Family: Embiotocidae) Urogenital Papillae

**Author: Angelina Guzman**
**Advisor: Kristy L. Forsgren**

### ABSTRACT

Surfperch (*Embiotocidae*) are costal marine fishes that live in the Pacific Ocean with one freshwater species in northern California. Surfperch are viviparous fishes; they copulate, go through internal fertilization, and the female gives live birth to young. Our lab has determined that all species of surfperch have an external urogenital papilla, the male intromittent organ (Bond and Forsgren 2021). During copulation, the males transfer sperm into the female reproductive tract via the urogenital papilla. The shape and size of the urogenital papilla appears to be diverse amongst Embiotocid species. I hypothesized that different species of surfperch will have different shaped and sized urogenital papillae. Three species from the subfamily Amphistichinae were examined: redtail surfperch (*Amphistichus rhodoterus*), walleye surfperch (*Hyperprosopon argenteum*), and silver surfperch (*Hyperprosopon ellipticum*) and five species from the subfamily Embiotocinae: white surfperch (*Phanerodon furcatus*), sharpnose seaperch (*Phanerodon atripes*), pile surfperch (*Phanerodon vacca*), rubberlip seaperch (*Rhacochilus toxotes*), and pink surfperch (*Zalembius rosaceus*). Macrophotography of museum specimens were used to investigate the size and shape of urogenital papillae (Bond and Forsgren 2021). Using MorphoJ (C. P. Klingenberg. 2011. MorphoJ: an integrated software package for geometric morphometrics. Molecular Ecology Resources 11: 353-357. doi: 10.1111/j.1755-0998.2010.02924.x), I obtained area measurements of the urogenital papilla for three individuals of each species with the exception of the sharpnose and rubberlip surfperches in which only two individuals were examined. I determined that surfperches have spherical-shaped urogenital papilla (redtail, sharpnose, pile, rubberlip, pink surfperches), while walleye and silver had crescent-shaped urogenital papilla, and white surfperch had triangular-shaped urogenital papilla (Fig. 1). Additionally, the urogenital papilla in the subfamily Amphistichinae had large, flattened papilla. Whereas for the Embiotocinae had smaller urogenital papilla and protruded more from the body. The size and shape of the urogenital papilla may be species-specific as well as aid in identification of conspecifics. Size and shape of the urogenital papilla may also be related to the habitat in which they occupy. A larger, more robust papilla might be necessary for species that experience high water turbulence whereas species that live in calmer waters may have smaller, flattened urogenital papilla. By examining the urogenital papilla of varies species of surfperches, it was determined that the shape and size does differ between the species. Overall, my research contributes to our understanding of the urogenital papilla in male surfperch reproductive biology and may provide insight into the reproductive morphology of other viviparous marine fishes.

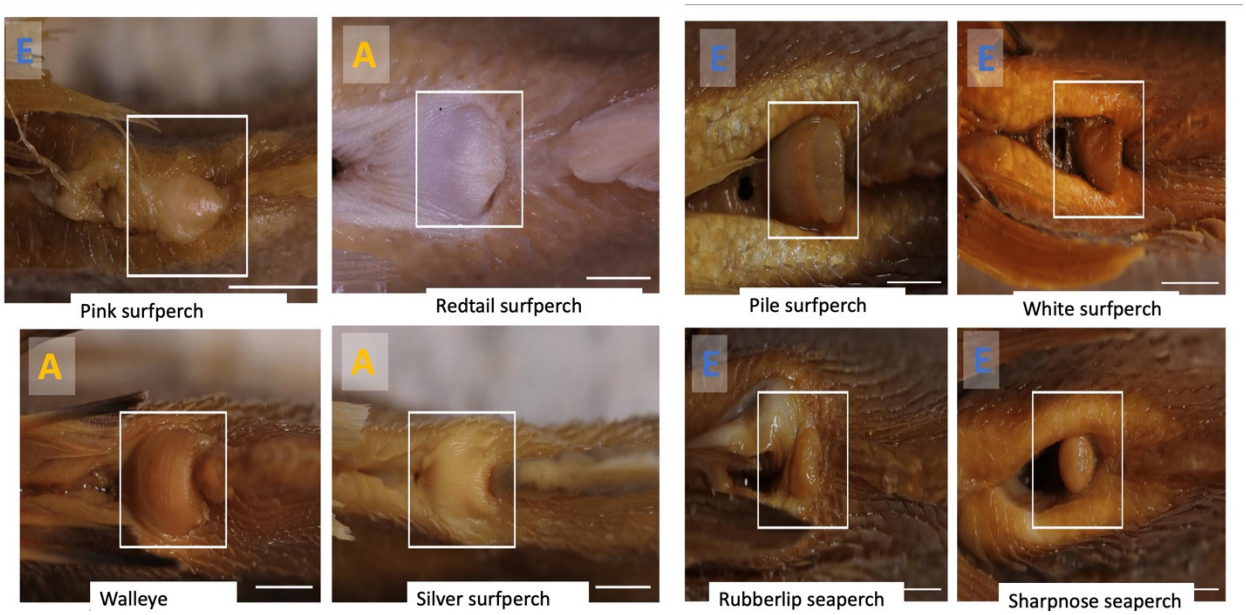


Figure 1. Photographs taken by Evelyn Bond (Bond and Forsgren 2021) of the urogenital papillae of all species worked on for this project; redtail surfperch (*Amphistichus rhodoterus*), walleye surfperch (*Hyperprosopon argenteum*), silver surfperch (*Hyperprosopon ellipticum*) white surfperch (*Phanerodon furcatus*), sharpnose seaperch (*Phanerodon atripes*), pile surfperch (*Phanerodon vacca*), rubberlip seaperch (*Rhacochilus toxotes*), and pink surfperch (*Zalembius rosaceus*). 'E' represents species from the subfamily Embiotocinae and 'A' indicates species from the subfamily Amphistichinae.

## LITERATURE CITED

Bond, ER., Forsgren, KL. 2021. External reproductive structures of male Surfperches (Embiotocidae): Urogenital papilla. The Anatomical Record DOI: 10.1002/ar.24836

# Rat carcass consumption as a pathway of secondary rodenticide exposure for wildlife in natural areas of southern California

**Author: Gabriela Guzman**
**Advisor: Paul Stapp**

## ABSTRACT

Anticoagulant rodenticides (ARs) are used to control rodent pest species and minimize damage to human property and disease spread. Their effectiveness and high usage have caused non-target wildlife species to be exposed to rodenticides. Species can consume ARs directly or may be exposed through the consumption of dead or dying animals (secondary exposure). The goal of my research project was to understand how non-target wildlife are secondarily exposed to ARs in natural areas of southern California. I deployed digital game cameras to determine the fate of 24 rat carcasses placed in three natural areas for seven consecutive days. I compared the rate of carcass removal to that from trials conducted in suburban backyards in the region (Lotts 2019). Of the 24 carcasses, 17 were removed (71%); similarly, Lotts (2019) reported a removal rate after seven days of 65% in suburban yards. I observed eight different scavenger species removing carcasses, including five mammals and three birds. By comparison, Lotts (2019) detected scavenging by seven different types of wildlife, with Virginia opossums and corvids the most common species. Although more carcasses were removed on the first day in suburban areas than natural areas (40% vs. 21%), overall, there was no significant difference between survival rates of carcasses in natural areas compared to suburban yards. These results help to better understand how non-target wildlife are exposed to ARs in suburban and wild areas.

**Keywords:** Anticoagulant rodenticides, Rat carcasses, Secondary poisoning, Scavenging

## BACKGROUND

Rodents are among the most successful species to cohabit with humans. Common commensal species include the house mouse (*Mus musculus*) and the brown and black rat (*Rattus norvegicus* and *R. rattus*, respectively). Commensal rodents have global impacts on food production, human health, and infrastructure (Elliott et al. 2016). To limit damage caused by these pests, humans developed anticoagulant rodenticides (ARs) to control rodent populations (Elliot et al. 2016). Anticoagulant rodenticides inhibit normal blood-clotting by disrupting the vitamin K cycle; they inhibit vitamin K epoxide reductase and alter cellular responses, damaging blood clotting mechanisms (Rattner et al. 2014). ARs developed between the 1940s and 1960s are called first-generation anticoagulant rodenticides (FGARs), whereas those developed between the 1970s and 1980s in response to increasing AR resistance are called second-generation anticoagulant rodenticides (SGARs). FGARs have a lower potency and must be ingested repeatedly to obtain a lethal dose (Erickson and Urban 2004). SGARs have higher toxicity than FGARs, and rodents can obtain a lethal dose after a single meal (Erickson and Urban 2004). However, rodents may continue to feed for several days, leading to the accumulation of large amount of rodenticide in the animal's kidneys, pancreas, and liver. Dead and dying rodents that are accessible to predators or scavengers represent a significant risk for AR exposure (Erickson and Urban 2004).

AR exposure pathways can be very complex, with potentially multiple levels of interaction. Routes

of transfer include primary, secondary, and tertiary exposure (Elliot et al. 2016). Primary exposure of ARs occurs when animals such as mice, rats, birds, and invertebrates consume AR bait directly. Secondary exposure occurs when predators or scavengers consume dead or dying prey, whereas tertiary exposure occurs when other predator species consume a secondarily exposed predator. Understanding the mode of exposure for non-target species is essential in implementing risk mitigation measures. There is a need for a better understanding of the route of exposure for non-target species and the extent to which AR poisoning travels up food chains (Elliot et al. 2016).

One approach to determining potential exposure associated with ARs is to examine the fate of carcasses placed in the environment and the species that consume them. For example, DeVault and Rhodes (2002), working in a forested landscape in Georgia, reported that 65% of rat and mouse carcasses were removed during a 2-week period, with a mean elapsed time of 5.6 days for carcass removal (DeVault and Rhodes 2002). To see whether predators and scavengers could be secondarily exposed to AR-contaminated carcasses in suburban environments, Lotts (2019) examined the rate of discovery of rat carcasses placed in residential backyards in southern California. Of the 20 rat carcasses he placed in different yards, 65% were removed by scavengers and carnivores within seven days (Lotts 2019). Seven different species removed carcasses, with 40% of carcasses partially or completely consumed within the first 24 hours (Lotts 2019).

Southern California is home to a diverse community of wildlife species that live at the urban-wildland interface and could become secondarily exposed to ARs applied there if they consume AR-killed or dying rodents that wandered into natural areas, or if they foraged in developed areas themselves. I predicted that the rate of carcass discovery and removal would be lower in natural areas than in suburban backyards (Lotts 2019), and more wildlife species will visit rat carcasses than reported in residential areas of southern California by Lotts (2019). I used digital game cameras to monitor the fates of 24 rat carcasses placed in three sites in Los Angeles and Orange County to determine if the wildlife species that scavenge these carcasses are different from those in suburban areas and if the discovery and removal rates differ.

## METHODS

### Study Areas

In much of southern California, areas of natural vegetation such as montane, grassland, riparian, and shrubland communities are interspersed with urban and suburban development. I studied the fates of rat carcasses in three natural areas: the Robert J. Bernard Field Station, in Los Angeles County, and the Starr Ranch Audubon Sanctuary, and Tucker Wildlife Sanctuary, both in Orange County.

A total of 24 carcasses of domestic rats were placed at the three areas: six were placed at the Bernard Field Station, in Claremont; seven at Tucker Wildlife Sanctuary, in Modjeska Canyon; and 11 at Starr Ranch Audubon Sanctuary, in Trabuco Canyon, in two separate trials (five and six carcasses). The predominant vegetation type at the locations where carcasses were placed was riparian woodland or coastal sage scrub, although all three sites also had non-native grasslands and some chaparral. Fieldwork was conducted in February and October 2020, during periods of clear, dry weather.

### Field Methods

Domestic rat carcasses (*R. norvegicus domestica*) were purchased from reptile pet food vendors (RodentPro.com; Amazon Reptile Center, Montclair, California) and stored frozen until used in trials. Between five and seven carcasses were placed at each site at a time. Carcasses were attached by cable ties to metal cables anchored to the ground, which required scavengers to spend time with the carcass, increasing the odds that they would be detected by cameras. Carcasses

were placed at least 200 m from each other, with an average distance of 490 m between adjacent carcasses, to reduce opportunities for predators to visit multiple carcasses. A Reconyx PC800 infrared digital camera strapped to a bucket was used to monitor animals visiting, interacting with, and removing carcasses. Cameras ran continuously, with images recorded every 5 seconds once the camera triggered. The cameras detected movements up to 30.5 m, but the range was dependent on the temperature of objects entering the camera field relative to ambient air temperature. Carcasses were monitored for seven consecutive days and then removed if they were still present.

**Image Analysis**

The images collected were classified based on the level of interaction between the visitors and carcass, using the approach of Lotts (2019). Images were placed into three categories (presence, interaction, removal) and the time, date, and visitor behavior was recorded. Presence was defined as any image showing any animal and the carcass together. Images showing obvious visitor awareness of the carcass (e.g., pawing, sniffing) were categorized as interaction. Removal was defined as the visitor breaking into the body cavity or physically removing the carcass, i.e., in such a way that it might be exposed to rodenticide if it was present in the carcass. All images, including those captured after the complete or partial removal of the carcass, were examined. Because cameras often recorded multiple images of the same individual, especially when it was removing the carcass, I assumed that images taken within 10 min of one another were the same individual visitor.

## RESULTS

Overall, a total of 26 different wildlife species visited the carcass locations, based on camera images: 13 mammals, 11 birds, and two reptiles (Table 1). Of the 24 carcasses, 22 (92%) were interacted with to some degree and 17 (71%) were wholly or partially removed within the seven-day period (Table 2; Fig. 1 and 2). Only one carcass (SRS4) was never visited by wildlife species. In all, eight different species wholly or partially removed carcasses, although California ground squirrels were the only species to partially consume a carcass without removing it. Mammals removed the most carcasses (10/17), with Virginia opossums responsible for most removals (5/17). Common Ravens, Turkey Vultures, and Red-shouldered Hawks removed four of the 17 carcasses (Table 2). All removals by birds occurred during the day, where all known removals by mammals except those by ground squirrels were detected at night. Due to camera malfunctions, images were not obtained for three of the carcasses that were removed (SR7, 8, 11; Table 2). The time of removal was assigned as the time of the first image taken without the carcass present; two of these occurred during the first 24 hours and one on the second day.

The fewest carcasses were removed from the Bernard Field Station; although multiple species investigated and interacted with carcasses, only one of the six carcasses was briefly chewed by a California ground squirrel (Table 2). All seven carcasses placed at the Tucker Wildlife Sanctuary were removed, whereas 10 of the 11 carcasses at the Starr Ranch were removed (Table 2). Birds, which are diurnal, tended to discover the carcasses more quickly, with one carcass removed by a Red-shouldered Hawk at Starr Ranch within 2 hours of placement.

I calculated Kaplan-Meier survival curves to describe carcasses' survival rates in natural and suburban locations (Fig. 3). Within the first day, five of the 24 (21%) carcasses from natural areas were removed, compared to eight of 20 (40%) residential carcasses. At the end of seven days, 17 of 24 (71%) natural carcasses had been removed, compared to 13 of 20 (65%) residential carcasses (Lotts 2019). Overall, however, survival curves were not significantly different from one another (log-rank test, $X^2 = 0.075$, d.f. = 1, P = 0.784). The median survival time for carcasses in natural areas was 4.0 days, compared to 4.5 days in suburban areas.

## DISCUSSION

Despite my prediction that the rate of carcass discovery and removal in natural areas would be lower than that in suburban areas, there was no significant difference in overall carcass removal rates between the areas (71% vs 65%). However, a greater variety of wildlife species did visit rat carcasses in natural areas. Natural areas lacked the barriers common in suburban yards, providing access to a wider variety of scavengers and predators (Table 2). It was common for the carcass to be discovered and removed by the same type of scavenger or predator (10/24 carcasses). Birds found carcasses the most quickly; on one occasion, a Red-shouldered Hawk removed a carcass within the first 2 hours (Table 2), a result that was similar to that reported by McTee et al. (2019). The Turkey Vulture and Common Raven also found the carcasses quickly. This shows the ability of birds, such as ravens, to use their large foraging radii to be efficient at locating carcasses (Lafferty et al. 2016).

Lotts (2019) reported that opossums removed the most carcasses, presumably because they can use trees and shrubs to climb over barriers in suburban backyards. In my study, opossums also removed the most carcasses (5/17) from natural areas, as expected by their abundant populations, as seen in a Midwestern study of carcass removal (Beasley et al. 2015). Similarly, birds removed the second-most carcasses in both natural and suburban locations. Lotts (2019) regularly detected crows and ravens, which are common corvids in suburban areas, but no larger birds of prey. I recorded two Red-Shouldered Hawks, one Turkey Vulture, and one Common Raven. High rates of carcass removal by birds, especially corvids, were expected for both wild and suburban areas because, unlike most mammals, they are not hindered by the barriers found in suburban areas. Of the four carcasses consumed by birds in natural locations, three were torn from the stakes and transported off camera. If these carcasses were not completely eaten, it is possible that they may have then been consumed by other unknown scavengers. Like Lotts (2019), in my study, I found arthropods in carcasses at the end of the seven-day trial period and both birds and mammals appeared to be eating these arthropods. Consumption of invertebrates can be another pathway for scavengers, as well as insectivores, to be secondarily exposed to ARs (Hoare and Hare 2006; Elliott et al. 2014).

The percentage of carcasses removed in my study (71%) is similar to the carcass removal rate reported by DeVault and Rhodes (2002; 65%). They reported that the highest removal rates occurred between the sixth and seventh day, while, in my study, daily rates of removal were generally similar across the first five days of my trials (Fig. 3). Conversely, Lotts (2019) observed the highest daily removal rate in the first 24 hours in suburban areas (40%). In my study, all of the first-day removals where the scavenger could be identified were by birds, whereas most (63%) of those detected by Lotts (2019) on the first day were mammals (opossums, coyote, cat). Taken together, these high removal rates indicate carcass consumption could be a considerable pathway for secondary AR exposure for wildlife, especially in suburban southern California.

The use of remotely triggered game cameras revealed a few limitations of my study. In three cases, carcasses were removed without any photographs. These instances occurred on very hot days, and failure to detect the motion of scavengers may have been caused by the lack of significant temperature difference between the environment and the scavenger. The presence of cameras themselves may have deterred scavenging. Coyotes and bobcats sometimes seemed wary of the cameras and did not approach carcass locations closely. Interestingly, two of the carcasses in Lotts' (2019) study were removed by coyotes, suggesting that coyotes in suburban areas may be habituated to carcasses, cameras, or other noisy or illuminated objects, and thus may be more opportunistic in consuming carcasses. Lotts (2019) recorded a bobcat interacting with one carcass, but saw no evidence of consumption; likewise, I recorded presence of bobcats at three carcass locations, but they visited after the carcasses had been taken by other scavengers, suggesting

that bobcats might be particularly wary. I also did not record presence of any mountain lions, even though they were known to be present and active at Starr Ranch and Tucker Wildlife Sanctuary. Both bobcats and mountain lions in southern California are known to be exposed to ARs at high rates (Moriarty et al. 2012, Serieys et al. 2015), but it is not clear exactly how this exposure occurs.

Prior to the application of ARs to control rodent pests, the potential risks of primary, secondary, and tertiary exposure of terrestrial and aquatic species should be considered. The California Department of Pesticide Regulation (DPR) attempted to mitigate AR exposure risk by restricting SGARs to only be purchased by certified pesticide applicators (CDPR 2018) and, in 2020, imposed a moratorium on nearly all applications of SGARs. As my results and those of Lotts (2019) demonstrate, there are many wildlife species in southern California capable of gaining access to ARs by consuming carcasses. To minimize this risk, those applying rodenticides should check for and remove rodent carcasses regularly to reduce opportunities for non-target exposure.

## ACKNOWLEDGMENTS

I want to thank Sandy and Pete DiSimone, Marcella Gilchrist, and Dr. Wallace M. Meyer III for giving me permission to use their lands for my experiments and for their advice. I would also like to thank all the Stapp lab members and a special thanks to Kaitlyn Berry for her assistance with the camera equipment and to Chris Burke for assistance with GIS maps. In addition, I am also thankful to Cindy Rojas and Tomas Nava for their support. Finally, I would like to thank Dr. Stapp for his unwavering support in helping me complete this project.

## LITERATURE CITED

Beasley, J. C., Z. H. Olson, N. Selva, and T. L. DeVault. 2019. Ecological functions of vertebrate scavenging. Pp. 125-157 in: Olea, P., Mateo-Tomás, P., Sánchez-Zapata, J. (eds) Carrion Ecology and Management. Wildlife Research Monographs, vol 2. Springer, Cham, Switzerland.

CDPR [California Department of Pesticide Regulations]. 2018. An investigation of anticoagulant rodenticide data submitted to the Department of Pesticide Regulation.

DeVault, T. L., and O. E. Rhodes. 2002. Identification of vertebrate scavengers of small mammal carcasses in a forested landscape. Acta Theriologica 47:185–192.

Elliot, J. E., S. Hindmarch, C. A. Albert, J. Emery, P. Mineau, and F. Maisonneuve. 2014. Exposure pathways of anticoagulant rodenticides to nontarget wildlife. Environmental Monitoring and Assessment 186:895-906.

Elliott, J. E., B. A. Rattner, R. F. Shore and N. W. V. D. Brink. 2016. Paying the pipers: mitigating the impact of anticoagulant rodenticides on predators and scavengers. BioScience 66:401–407.

Erickson, W., and D. Urban. 2004. Potential risks of nine rodenticides to birds and non-target mammals: A comparative approach. United States Environmental Protection Agency, Office of Prevention, Pesticides and Toxic Substance. Washington, D.C., USA.

Hoare, J. M., and K. M. Hare. 2006. The impact of brodifacoum on non-target wildlife: gaps in knowledge. New Zealand Journal of Ecology 30:157-167.

Lafferty, D. J., Z. G. Loman, K. S. White, A. T. Morzillo, and J. L. Belant. 2016. Moose (*Alces alces*) hunters subsidize the scavenger community in Alaska. Polar Biology 39:639-647.

Lotts, B. 2019. Consumption of rat carcasses as a pathway of rodenticide exposure of wildlife in suburban Orange County. Project Report, Master of Science in Environmental Studies, California State University Fullerton.

Mackenzie, J. S., M. Jeggo, P. Daszak, and A. Richt Jürgen A. 2016. One Health: The human-animal-environment interfaces in emerging infectious diseases food safety and security, and international and national plans for implementation of one health activities. Springer Berlin, Berlin.

McTee, M., B. Hiller, and P. Ramsey. 2019. Free lunch, may contain lead: scavenging shot small mammals. Journal of Wildlife Management 83:1466-1473.

Moriarty, J. G., S. P. D. Riley, L. E. Serieys, J. A. Sikich, C. M. Schoonmaker, and R. H. Poppenga. 2012. Exposure of wildlife to anticoagulant rodenticides at Santa Monica Mountains National Recreation Area: From mountain lions to rodents. Pp. 144-148 in: Timm, R. M. (ed)

Proceedings of the 25th Vertebrate Pest Conference. Davis, California, USA.

Rattner, B. A., R. S. Lazarus, J. E. Elliott, R. F. Shore, and N. V. D. Brink. 2014. Adverse

outcome pathway and risks of anticoagulant rodenticides to predatory wildlife. Environmental Science & Technology 48:8433–8445.

Reconyx Inc. 2013. Hyperfire high performance cameras: Hyperfire instruction manual. Holmen, Wisconsin, USA.

Serieys, L.E., T. C. Armenta, J. G. Moriarty, E. E. Boydston, L. M. Lyren, R. H. Poppenga, K. R. Crooks, R. K. Wayne, and S. P. Riley. 2015. Anticoagulant rodenticides in urban bobcats: exposure, risk factors and potential effects based on a 16-year study. Ecotoxicology 24:844-862.

**Table 1.** *Wildlife species photographed at rat carcasses in three sites with natural vegetation in southern California between February and October 2020. One Reconyx digital camera monitored activity continuously at each carcass for seven consecutive days. Abbreviations are used in Table 2.*

| **Common name** | **Species name** | **Abbreviation** |
|---|---|---|
| Virginia opossum | *Didelphis virginiana* | DIVI |
| Desert cottontail | *Sylvilagus audubonii* | SYAU |
| California ground squirrel | *Otospermophilus beecheyi* | OTBE |
| Pacific kangaroo rat | *Dipodomys agilis* | DIAG |
| Deer mouse | *Peromyscus* spp. | PESP |
| Big-eared woodrat | *Neotoma macrotis* | NEMA |
| Coyote | *Canis latrans* | CALA |
| California grey fox | *Urocyon cinereoargenteus* | URCI |
| Raccoon | *Procyon lotor* | PRLO |
| Striped skunk | *Mephitis mephitis* | MEME |
| Bobcat | *Lynx rufus* | LYRU |
| Domestic cat | *Felis catus* | FECA |
| Mule deer | *Odocoileus hemionus* | ODHE |
| Southern Pacific rattlesnake | *Crotalus helleri* | CRHE |
| Western fence lizard | *Sceloporus occidentalis* | SCOC |
| Spotted Towhee | *Pipilo maculatus* | SPTO |
| California Thrasher | *Toxostoma redivivum* | CATH |
| California Scrub-Jay | *Aphelocoma californica* | CASC |
| California Quail | *Callipepla californica* | CAQU |
| Common Raven | *Corvus corax* | CORA |
| Turkey Vulture | *Cathartes aura* | TUVU |
| Red-shouldered Hawk | *Buteo lineatus* | RSHA |
| White-crowned Sparrow | *Zonotrichia leucophrys* | WCSP |
| Northern Flicker | *Colaptes auratus* | NOFL |
| California Towhee | *Melozone crissalis* | CATO |
| Mourning Dove | *Zenaida macroura* | MODO |

**Table 2.** *Summary of visitation of wildlife species to rat carcasses placed at three sites (Bernard Field Station, BFS; Tucker Wildlife Sanctuary, TS; Starr Ranch Audubon Sanctuary, SRS) with natural vegetation in southern California. See Table 1 for species codes. UNK = unknown species removed carcass. Interaction and Presence columns list the first species interacting with or photographed with the carcass; subsequent visitors and the total number of images of each species taken are listed in the right-most column.*

| Site | Camera No. | Removal | Interaction | Presence | Other Visitors-Number of images captured |
|---|---|---|---|---|---|
| BFS | 7 | - | OTBE 4 h | OTBE 2 h | NEMA-90, SYAU-97, OTBE-65, CALA-3 |
| BFS | 8 | OTBE 124 h | CATO 1 h | CATO 1 h | PEMA-31, SYAU-20, OTBE-10, NEMA-15, CATO-55 |
| BFS | 9 | - | NEMA 140 h | OTBE 3 h | NEMA-142, SYAU-86, OTBE-95, WCSP-17, DIAG-5, CATO-15 |
| BFS | 10 | - | PEMA 35 h | CATO 23 h | PEMA-35, SYAU-15, OTBE-15, NEMA-41, CATO-15, CATH-15 |
| BFS | 11 | - | - | SYAU 18 h | SYAU-5 |
| BFS | 12 | - | CASC 2 h | CATO 1 h | PEMA-10, SYAU-379, OTBE-149, NEMA-65, CATO-65, CATH-65, DIAG-213, CASC-20, WCSP-15, MODO-5, SPTO-3 |
| TS | 7 | MEME 32 h | DIAG 30 h | PEMA 26 h | PEMA-10, MEME-10, WCSP-50, CATO-15, URCI-5, CRHE-5 |
| TS | 8 | DIVI 56 h | - | WCSP 16 h | PEMA-15, MEME-40, WCSP-10, URCI-10, OTBE-1, CATH-5, SPTO-5, DIVI-55 |
| TS | 9 | URCI 60 h | CASC 25 h | LYRU 10 h | PEMA-1, MEME-95, CATO-5, CASC-65, URCI-110, SYAU-25, FECA-80, LYRU-5, CAQU-17 |
| TS | 10 | CORA 19 h | - | CATH 1 h | PEMA-55, CATH-25, WCSP-15, URCI-40, NEMA-5, CORA-5, NOFL-25, TUVU-90, SYAU-25 |
| TS | 11 | PRLO 103 h | - | PEMA 10 h | PEMA-30, PRLO-5, CATO-5 |
| TS | 12 | TUVU 21 h | - | - | PEMA-30, TUVU-20, URCI-102, |
| TS | 13 | DIVI 30 h | NEMA 27 h | PEMA 28 h | PEMA-106, NEMA-1, CATO-15, CATH-9, URCI-60, DIVI-15 |
| SRS | 2 | DIVI 76 h | - | WCSP 14 h | PEMA-25, CATO-25, CASC-25, CATH-30, SPTO-15, LYRU-15, DIAG-55, WCSP-20, DIVI-47, URCI-65 |
| SRS | 3 | DIVI 79 h | - | - | DIVI-19 |
| SRS | 4 | - | - | - | - |
| SRS | 5 | DIVI 108 h | - | - | DIVI-67 |
| SRS | 6 | RSHA 95 h | - | - | RSHA-31, CALA-6, CATO-6 |
| SRS | 7 | UNK 18 h | - | - | PEMA-5, CATO-10, DIAG-30, MEME-5 |
| SRS | 8 | UNK 39 h | - | - | PEMA-5, LYRU-10, ODHE-10, CATH-20 |
| SRS | 9 | - | SCOC 5 h | SPTO 22 h | SPTO-15, NEMA-20 |
| SRS | 11 | UNK 18 h | - | - | MEME-15 |
| SRS | 12 | MEME 109 h | - | - | MEME-20 |
| SRS | 13 | RSHA 2 h | - | - | |


**Figure 1.** *Images of wild mammals that removed carcasses at Tucker Wildlife Sanctuary (A-D), Starr Ranch Sanctuary (E-H), and Bernard Field Station (I): (A) Virginia opossum; (B) Virginia opossum; (C) Virginia opossum; (D) raccoon; (E) striped skunk; (F) California grey fox; (G) Virginia opossum; (H) California ground squirrel.*


**Figure 2.** *Images of wild birds removing carcasses at Tucker Wildlife Sanctuary (A-B) and Starr Ranch Sanctuary (C-D): (A) Common Raven; (B) Turkey Vulture; (C) Red-shouldered Hawk; (D) Red-shouldered Hawk.*

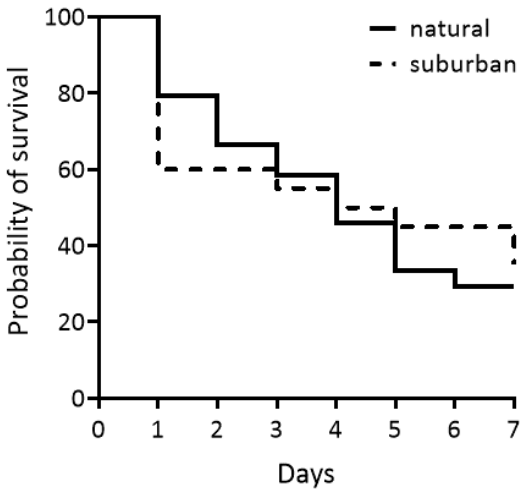


**Figure 3.** *Comparison of rates of removal, depicted here as Kaplan-Meier survival curves, of rat carcasses placed in natural areas (N = 24) and suburban backyards [(N = 20); data from Lotts (2019)] in southern California over 7-day trials.*

## Whydah you follow Munias around? Pin-Tailed Whydah population growth in Southern California, tracks that of potential brood host, the Scaly-Breasted Munia

**Author: Alisa Hernandez**
**Advisor: William J. Hoese**

### ABSTRACT

Pin-tailed whydahs, (*Vidua macroura*), are obligate, avian brood parasites that lay their eggs in the nests of host birds. Introduced from Africa via the pet trade, whydah sightings in southern California have increased since the 1990s and a local breeding population has been established. Brood parasites often negatively affect the reproductive success of their hosts, thus understanding how whydahs have been successful in California is crucial for protecting local bird populations. One potential host of the whydah is the scaly-breasted munia (*Lonchura punctulata*). The munia is closely related to African whydah hosts yet is native to Asia; it also escaped the pet-trade in southern California and established a breeding population in the 1990s. I hypothesized that whydahs would use munias as hosts and predicted that the whydah population would be positively correlated with the munia population. With georeferenced data from databases, I mapped known locations of whydahs and munias in southern California to document the geographic range expansion of both species. Sightings across southern California of both species have increased exponentially since 2000. These correlational results suggest that munias may serve as brood hosts for whydah nestlings. Future work will survey munia nests to confirm their role as whydah hosts. The use of other hosts and resources, such as habitat type and seed availability may also contribute to the whydah's success in southern California. Brood parasites cause host reproductive success to suffer, and the pin-tailed whydah may represent a new threat to local bird species.

## Influence of the Microbiota on Host Phenotypes in *Drosophila melanogaster*

**Author: Michaelangelo Marcellana**
**Advisor: Parvin Shahrestani**

### ABSTRACT

The interaction between microbiota and hosts is an active area of investigation. Laboratory selection, in which model organisms are evolved for different traits, is a useful tool to study the impact of the microbiota on the host and vice versa. The genetic model organism *Drosophila melanogaster*, laboratory fruit fly, has short generation times and is affordable and easy to maintain, making it a suitable model for laboratory selection studies. In accordance with the evolutionary theory of aging, experimentally manipulating the age of first reproduction in a population (a form of laboratory selection) leads to divergence in aging patterns and in longevity (Rose et al., 2004). This evolved longevity differentiation is accompanied by divergence in other traits, including desiccation and starvation resistance, reproductive output, and developmental rate (Rose et al., 2004). Recently, our laboratory has shown that the evolved longevity differentiation is also accompanied by changes to the microbiota (Figure 1). The *D. melanogaster* microbiota is primarily made up of lactic acid (LAB) and acetic acid (AAB) bacteria, including *Lactobacillus* and *Acetobacter*, respectively. Specifically, through analyzing whole-genome sequences for the A- and C- type populations, we found that the endosymbiont *Wolbachia* was absent in almost all A-types but was prevalent in all C-types (Figure 1A). These differences are visible after hundreds of generations of selection (LS) and also after only dozens of generations of selection (Int) (Figure 1A). Analysis of 16S rRNA marker gene sequences further confirmed the absence of *Wolbachia* in the A-type populations (Figure 1B). Through plating homogenized flies and counting colony-forming units, we showed that the absolute abundance of both LAB and AAB were higher in A-types compared to C-types (Figure 1C). Lastly, we identified host genetic control of the microbiota; when both A-type and C-type flies were made bacteria-free and given controlled doses of bacteria, the bacteria grew to higher abundances in A-type hosts (Figure 1D). Our preliminary results show that host evolution affects the microbiota and raises the question of whether the microbiota exerts influence on host evolution. We are developing techniques to evolve fly populations for changes in the first age of reproduction under bacteria-controlled conditions in order to study the impact of the microbiota on the host rate of evolution.

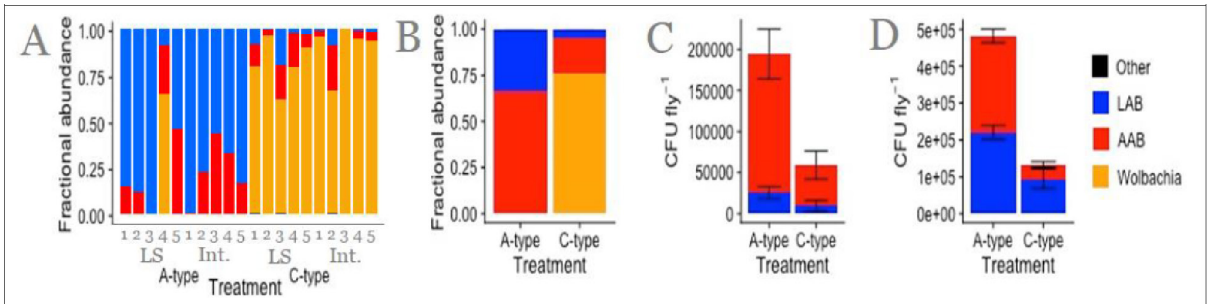


**Figure 1.** Bacterial composition and abundance in A- and C-types. A) MetaPhlAn2 was used for read matching from whole-genome sequence data. C-types have higher fractional abundance of *Wolbachia* than A types and within A types LAB are more frequent than AAB (p values <0.05). B) 16S rRNA V4 marker gene sequencing of whole body flies both supports and contradicts results of panel A (N = 2 reps per line, 5 lines per treatment, 2 expts). CFU counts of C) conventional flies (N = 10 reps per line, 5 lines per treatment, 1 expt) and D) 5-species gnotobiotic (N = 2 reps per line, 5 lines per treatment, 3 expts). Kruskal-Wallis chi-squared tests comparing total CFUs, LAB, and AAB in panels B and C reveal that A-types have higher total, LAB, and AAB abundances of bacteria than C-types (all p-values < 0.002).

## REFERENCES

Rose, M. R., Passananti, H. B., & Matos, M. (Eds.). (2004). Methuselah flies: a case study in the evolution of aging. World scientific.

## ACKNOWLEDGEMENTS

Collaborator Dr. John Chaston from BYU. Current and former Shahrestani lab students, especially Robert Courville and Courtney Mueller.

# EFFECTS OF A NON-INDIGENOUS BRYOZOAN ON THE RECRUITMENT OF THE NATIVE OLYMPIA OYSTER, OSTREA LURIDA

**Authors: Leeza-Marie Rodriguez and Valerie Goodwin**
**Advisor: Danielle C. Zacherl**

## ABSTRACT

Non-indigenous fouling organisms settling onto artificial and natural hard substrata in estuaries can negatively impact native species via space competition, predation, or other mechanisms. The effects of *Amathia verticillata* and other fouling organisms on the recruitment of *Ostrea lurida* were studied to determine how its presence affects oyster growth, percent cover, and abundance. Terracotta tiles (0.15 meters x 0.15 meters) acted as proxies for available hard substrata, and were deployed on PVC tees in Upper Newport Bay, California at tidal elevations between -0.152 and -0.304 m MLLW in March 2021 during the spawning season of the oysters. Each tile replicate consisted of two tiles cemented together using marine epoxy with a layer of gardening mesh between the two tiles to provide netting that allowed for suspension of the tiles from each tee. Four treatment groups (N =10 replicate tiles) were established and maintained to examine the effects of *A. verticillata* and encrusting fouling species on *O. lurida* recruitment. The treatments were as follows: (1) unmanipulated controls (hereafter "Control"), (2) *A. verticillata* removals [(-) Amathia], (3) *A. verticillata* and encrusting fouler removals [(-) All], and (4) encrusting fouler removals [(-) Foulers]. The treatment groups were maintained by removing *A. verticillata* and encrusting foulers approximately once per month based on treatment. The replicates were arrayed alongshore across approximately 50 meters of shoreline. Once removed each month, *A. verticillata* and encrusting foulers were each measured for volume displacement as a proxy for biomass. Tiles were retrieved from the field in October 2022. *O. lurida* recruiting to the tiles were counted and measured for length and width. Species identification was confirmed via visual inspection for chomata on the interior of the shell near the hinge (Polson et al 2009). Percent cover was quantified using a 100 point contact technique for all encrusting invertebrate species that recruited to the tiles. Results suggest that *A. verticillata* might be influencing *O. lurida* recruitment in specific locations along the shoreline. Some non-indigenous fouling organisms may not be as problematic as predicted when restoring native species in estuarine communities.

# Geological Sciences

# Exploring the Evidence for Pluton Emplacement Mechanisms in the Jackass Lakes Pluton, California

**Author: Brandon Cugini**
**Advisor: Valbone Memeti**

## ABSTRACT

Emplacement of plutons is a common feature along convergent plate boundaries, and is integral for new crust generation. However, the mechanisms by which plutons are emplaced in magmatic arcs are still poorly understood, and have puzzled geologists for over 200 years. It is understood that in order for magma to move into the crust, space has to be made by shuffling around the host rock. Geologists rely on field observations of known plutons that outcrop on the surface to gather insight into their formation history. In this study, the Cretaceous Jackass Lakes Pluton will be examined to study its history of emplacement.

The pluton is located in the central Sierra Nevada Mountains in eastern California, and displays mineral fabrics that hint at a complicated history of formation. One of the first studies (McNulty et al. 1996) concluded that the magma body was emplaced through a combination of fracture propagation, stoping of wall and roof rock, and diking. Wiebe et al. (1999, 2000) concluded that the Jackass Lakes Pluton was emplaced by many mafic sills into felsic magma and subsequent tilting after magma crystallization. A more recent study by Pignotta et al. (2010) stated that the JLP was emplaced gradually and rapidly through diapirism with ductile deformation of its host rocks, downward return flow, diking, and widespread stoping. This conclusion agrees mostly with McNulty et al. (1996), but challenges Wiebe et al. (1999, 2000). What the past work agrees on is that multiple mechanisms are needed for pluton emplacement.

The aim of this study is to test the hypotheses of emplacement mechanisms through field investigations and examination of microstructures from rock fragments to look for evidence of different emplacement mechanisms. The regions along the boundaries of the JLP and the metavolcanic host rock will be examined since the evidence for pluton-wall rock relations were created and are preserved there. Moreover, the JLP is surrounded to the north and south by younger plutons, thus the field work will be restricted to the east and west boundaries where its intrusive contact with an older pluton is preserved. Evidence for emplacement include isolated wall rock pedants surrounded by pluton rock for stoping, long fissures and magmatic sheets of pluton rock for fracture propagation and diking respectively, subvertical host rock orientations for downward host rock displacement, and mineral foliation patterns and fabrics with respect to internal pluton contacts for downward return flow of magma.

# Using plagioclase geochemistry to examine the degree of magma mixing between the Kuna Crest sheeted complex and lobe magmas during the initiation of magmatism in the Tuolumne Intrusive Complex, California

**Author: Vincent Mugica**
**Advisor: Valbone Memeti**

## ABSTRACT

Magmatic mobilization and ascent from the upper mantle and lower crust through the arc crust and the degree to which these magmas are interconnected and mix with one another at different scales is an essential question of igneous petrology. Previous studies of large composite, compositionally zoned batholiths, such as the ~95 - 85 Ma, 1,100 $km^2$ Tuolumne Intrusive Complex, Sierra Nevada, California, demonstrate that batholiths are formed by incrementally emplaced batches of magma. These magmas undergo dynamic evolutionary mixing processes in magma mush systems as they progress through the crustal column that are recorded in plagioclase ($CaAl_2Si_2O_8$-$NaAlSi_3O_8$), a liquidus phase. This study seeks to understand the extent and nature of these mixing processes at the initiation of the Tuolumne Intrusive Complex, which is represented by the mafic, isotopically more mantle-like, 80 $km^2$ Kuna Crest Lobe and related sheeted complexes located in the southeastern domain of the Tuolumne Intrusive Complex.

We present geologic maps of the lithology and spatial relations of the Kuna Crest Lobe and its related sheeted zones at Marie Lakes and Gaylor Ridge, thin section size cathodoluminescence images to highlight zoning in plagioclase populations, optical petrography, and electron probe microanalysis and laser ablation-inductively coupled plasma-mass spectrometry element geochemistry to conclude the following: (1) All plagioclase grains assessed have anorthite contents ranging from $An_{37}$ to $An_{88}$. (2) Overall, plagioclase grains collected from the Kuna Crest Lobe show trace element ranges of Sr at 500 ppm – 1250 ppm commensurate with plagioclase grains collected from Gaylor Ridge, while plagioclase grains collected from the Marie Lakes sheeted zone have typically higher Sr signals at 900-1500 ppm. (4) Plagioclase grains analyzed from the Kuna Crest Lobe, Gaylor Ridge and Marie Lakes sheeted zones display heterogenous intra-unit profiles in Sr and Ba (ppm) versus anorthite space, which show at least 2 distinct populations of plagioclase in each of the lithologic subdomains and are different from one another.

We interpret these data as evidence that the embryonic construction of the Tuolumne Intrusive Complex occurred with the Kuna Crest Lobe and related sheeted complex magmas that already underwent magma mixing and were sourced from different magma bodies stored in a complex magma mush network in the crust prior to emplacement.

## The Volcanic-Plutonic Connection in the Jackass Lakes Pluton

**Author: Ashleigh Quiroz**
**Advisor: Valbone Memeti**

### ABSTRACT

The Jackass Lakes pluton (JLP) is a middle-Cretaceous composite pluton in the central Sierra Nevada of California that intruded into roughly coeval volcanic host rocks. Plutons that preserve related volcanic materials are rare, making the JLP a great place to study the volcanic-plutonic connection. The two endmember models are that volcanic rocks are either equivalent (both formed with the exact same composition) or complementary (where the volcanic plus plutonic rocks equal the original magma composition) to plutonic rocks. In order to examine such petrologic connections, one must first ascertain which volcanic and plutonic rocks are of the same age, which is the focus of this study.

While geochronologic data for the JLP exist, the data is sparse. Using $^{206}Pb/^{238}U$ zircon dating, Stern et al. (1981) first dated the JLP to 98 Ma. Volcanic rocks more centrally located to the JLP were dated ca. 99-101 Ma (Stern et al., 1981), while to the eastern border volcanic rocks were dated ca. 132–144 Ma (Fiske and Tobisch, 1994). Later, McNulty et al. (1996) refined the ages of the JLP via two samples: one from the northeast and the other from the southwest of the JLP. Implementing the same type of U-Pb zircon dating, they found that the northeastern JLP sample was 98.5 ± 0.3 Ma while the southwestern sample was slightly younger at 97.1 ± 1.1 Ma (McNulty et al. 1996). A more thorough geochronologic (and petrologic) study of the JLP and its volcanic pendants has yet to be done.

This study seeks to demystify the timeline of formation and evolution of the JLP plutonic and volcanic rocks as well as the timing of formation relative to one another, so ultimately a petrologic investigation can be completed. Implementing U-Pb zircon geochronology, a team of mappers will collect field samples from the JLP, taking three to four samples of each volcanic and plutonic units to understand better the order of formation between rhyolites and andesites and granodiorites and diorites present at the site. At CSUF, these samples will be cut and crushed, zircon crystals will be separated using a Frantz magnetic separator and heavy liquids, and readied to be taken to the Arizona LaserChron Center at the University of Arizona to analyze with the LA-ICP-MS.

## REFERENCES

Fiske, R. S., and Tobisch, O. T., 1994, Middle Cretaceous volcanic rocks in the Minarets caldera, east-central Sierra Nevada, California: Geological Society of America Bulletin, v. 106, 582–593 p.

McNulty, B.A., Tong, W., and Tobisch, O.T., 1996; Assembly of a dike-fed magma chamber; the Jackass Lakes Pluton, central Sierra Nevada, California: Geological Society of America Bulletin, v. 108, 926–940 p.

Pignotta, S.R. Paterson, C.C. Coyne, J.L. Anderson, J. Onezime, 2010; Processes involved during incremental growth of the Jackass Lakes pluton, central Sierra Nevada batholith. Geosphere, v. 6, 130–159 p.

Stern, T. W., Bateman, P. C., Morgan, B. A., Newell, M. F., and Peck, D. L., 1981, Isotopic U-Pb ages of zircon from the granitoids of the central Sierra Nevada, California: U.S. Geological Survey Professional Paper 1185, 17 p.

## Using Charcoal to Reconstruct a Fire History of the Carrizo Plains, CA

**Author: Dahlia Serrato**
**Advisor: Dr. Matthew Kirby**

### ABSTRACT

Southern California is characterized by a distinct fire season. The destruction forest fires wreak is profound, though the paleohistory of fires is poorly documented in Southern California. This study aims to reconstruct the first fire history of the Carrizo Plains National Monument to increase understanding of the conditions that cause fire activity in the past and provide knowledge of present and future fire activity. The Carrizo Plains are located roughly 85 miles north of Santa Barbara adjacent to the San Andreas Fault Zone. Core CLPC21-4 was extracted from a dry lakebed (34 59'31.0" N, 119 29'00.4 W) selected for its ability to collect water from the surrounding area. Fire activity was measured by quantifying woody and grassland charcoal extracted from 30-156 cm of core CLPC21-4. Sediment was extracted in 1 $cm^3$ increments and washed with deionized water of extraneous debris smaller than 125 μm. Charcoal was identified and recorded manually by binocular light microscope. Results shows an increase in charcoal at three points in the core, a period of very sparse charcoal, and variable fluctuations elsewhere. In combination with visual interpretation of the sediment, the peaks can be inferred as charcoal deposition due to flood events rather than true accounts of fire. Quantities of charcoal following these events are indicative of greater fire activity likely due to an increase in vegetation as fuel during wetter climate regimes. No conclusions can be drawn as to whether the period of low charcoal counts was a result of dampened fire activity or poor charcoal preservation due to drier climates. Further geochemical and physical analyses will provide greater insight into the complex history of the area.

# Mathematics

# Exploring classical guitar playing techniques through signal processing

Victor H. Sanchez
Advisor: Kristin M. Kurianski, Ph.D.

**Abstract**

We study the relationship between the plucking location along a guitar string and the strength of the harmonics in the resulting audio signal from both theoretical and experimental perspectives. The audio signal produced by plucking an acoustic guitar string at various locations was analyzed using the discrete Fourier transform. We then compare the resulting experimental data to the magnitude of the Fourier coefficients predicted by a theoretical model based on the one-dimensional wave equation.

## 1 Introduction

Classical guitarists use variations in plucking location to manipulate the tonal quality of the sound produced. Plucking near the center of the string (*sol tasto*) produces a rich tonal quality, while plucking near the endpoints of the string (*sol ponticello*) produces a harsh tonal quality [5, 6]. The tones produced are comprised of a fundamental frequency along with subsequent harmonics, which are integer multiples of the fundamental. The fundamental frequency is the predominant sound we hear and gives the tone its overall pitch. The higher harmonics present in the sound determine the quality of the tone. When higher harmonics are present in greater strength, the tone sounds bright or harsh. Conversely, when higher harmonics are diminished, the tone sounds warm or rich owing to the dominance of the fundamental.

Hughes (2000) presented mathematical rationale for the effects of plucking location on tonal quality using the one-dimensional wave equation [5]. They considered a simplified model of a plucked string as a piecewise linear function, given by

$$\tilde{f}_\alpha(x) = \begin{cases} \frac{\epsilon}{\alpha} x & 0 \le x \le \alpha \\ \frac{-\epsilon}{\pi - \alpha}(x - \pi) & \alpha < x \le \pi \end{cases} \tag{1}$$

for a string of length $\pi$, maximum vertical displacement $\epsilon$, and plucking location $\alpha$ [5].

The magnitude of the Fourier coefficients of $\tilde{f}_\alpha(x)$ are given by

$$|\tilde{a}_{n,\alpha}| = \frac{2\epsilon|\sin(n\alpha)|}{\alpha n^2(\pi-\alpha)} \tag{2}$$

as described in [5]. Upon graphing $|\tilde{a}_{n,\alpha}|$ for various $n$, Hughes (2000) noted that the plucking location $\alpha = \pi/2$ coincides with the maximum amplitude of the Fourier coefficient of the fundamental frequency $n = 1$ [5]. Moreover, this position also coincides with the even harmonics achieving zero amplitude and the odd harmonics remaining relatively small, accounting for the rich tonal quality of *sol tasto*. However, plucking locations near the endpoints coincide with a decreasing strength of the fundamental frequency and increases in the amplitudes of $|\tilde{a}_{n,\alpha}|$ for $n > 1$, accounting for the bright tonal quality of *sol ponticello* [5]. Hughes (2000) concludes with a note that it would be interesting to test this model using a real guitar, which is the focus of this paper.

## 2 Mathematical Model

Based on (1), we consider a generalized initial profile to describe a string of length $L$ and plucking location $\alpha$. The resulting profile has the form

$$f_\alpha(x) = \begin{cases} \dfrac{\epsilon}{\alpha}x & 0 \le x \le \alpha \\ \dfrac{-\epsilon}{L-\alpha}(x-L) & \alpha < x \le L \end{cases}, \tag{3}$$

an example of which is shown in Figure 1.

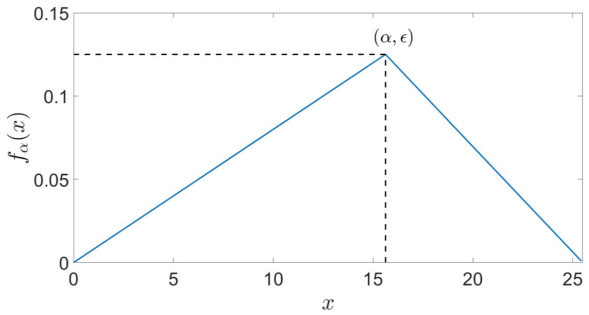


Figure 1: Example of initial profile for a string of length $L = 25$ plucked at location $\alpha = 15.625$ to a height of $\epsilon = 0.125$. All lengths are measured in inches.

The following model and resulting solution can be derived from standard computations found in many texts, for instance, [1, 3]. The motion of a vibrating string with fixed

endpoints can be modeled by the one-dimensional wave equation given by

$$\frac{\partial^2 u}{\partial t^2} = c^2 \frac{\partial^2 u}{\partial x^2} \tag{4}$$

where $u(x,t)$ is the amplitude of the string, $x$ is the spatial variable, $t$ is time, and $c$ is a constant related to the physical properties of the string. The boundary conditions for a string with fixed endpoints are given by

$$\begin{aligned} u(0,t) &= 0 \\ u(L,t) &= 0 \end{aligned} \tag{5}$$

and the initial conditions for our model are prescribed by

$$\begin{aligned} u(x,0) &= f_\alpha(x) \\ u_t(x,0) &= 0 \end{aligned} \tag{6}$$

where $f_\alpha(x)$ is given by (3) and $u_t$ denotes the partial derivative of $u$ with respect to $t$. Using separation of variables and applying conditions (5) and (6) leads to

$$u(x,t) = \sum_{n=1}^{\infty} a_{n,\alpha} \cos\left(\frac{n\pi c}{L} t\right) \sin\left(\frac{n\pi}{L} x\right) \tag{7}$$

where

$$a_{n,\alpha} = \frac{2}{L} \int_0^L f_\alpha(x) \sin\left(\frac{n\pi}{L} x\right). \tag{8}$$

Since we are interested in the strength of the amplitude of each respective mode in the sum given by (7) and its dependence on the plucking location $\alpha$, we consider the absolute value of (8) given by

$$|a_{n,\alpha}| = \frac{2\epsilon |\sin(n\pi\alpha/L)|}{\alpha(n\pi/L)^2(L-\alpha)} \tag{9}$$

where $\alpha < L$. Note that (9) reduces to (2) when $L = \pi$.

A plot of several theoretical Fourier coefficient amplitudes and their dependence on plucking location $\alpha$ are shown in Figure 2. Each curve corresponds to $|a_{n,\alpha}|$ for a given value of $n$. For example, the curve corresponding to $|a_{1,\alpha}|$ is labeled $n = 1$ and shows the amplitude of the Fourier coefficient of the fundamental frequency as a function of plucking location. Hughes (2000) presented a similar plot, although ours corresponds to a string of length $L = 25$ plucked at a height of $\epsilon = 0.125$, with lengths measured in inches. Note that the fundamental frequency has greatest amplitude when the string is plucked near $\alpha = 12.5 = L/2$, and the coefficients of higher harmonics have increased amplitude when plucked near the endpoints $\alpha = 0$ and $\alpha = 25$. This is consistent with Hughes' observation that the warm tones of *sol tasto* and the harsh tones of *sol ponticello* correspond to the relative Fourier coefficient amplitudes of the fundamental frequency and the overtones (i.e., higher harmonics) [5].

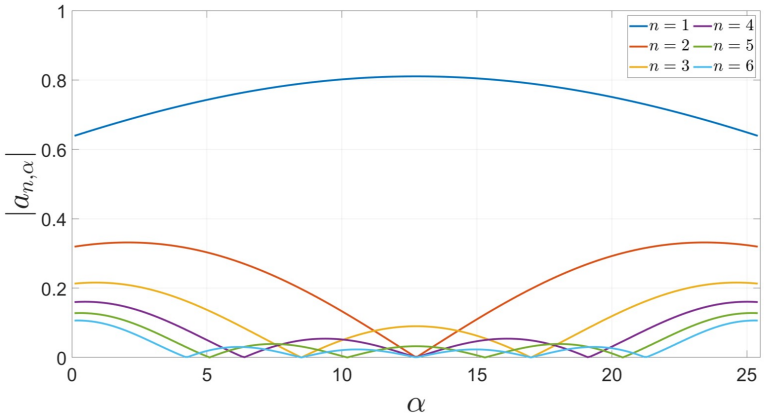


Figure 2: Magnitude of Fourier coefficients $a_{n,\alpha}$ as a function of plucking location $\alpha$ for $n = 1, 2, 3, 4, 5, 6$.

# 3 Experimental Implementation

## 3.1 Data Collection

We recorded the sound produced by the D string of an acoustic guitar picked or plucked at various locations. The guitar used was a JB Player JBEA35BK Acoustic Electric Guitar with Ernie Ball Super Slinky Classic Pure Nickel Electric Guitar Strings (9-42 Gauge) in standard tuning. The plucking locations were determined by measuring 15 equally-spaced points along the guitar string starting at the bridge (Figure 3). The measurements are given by Table 1.

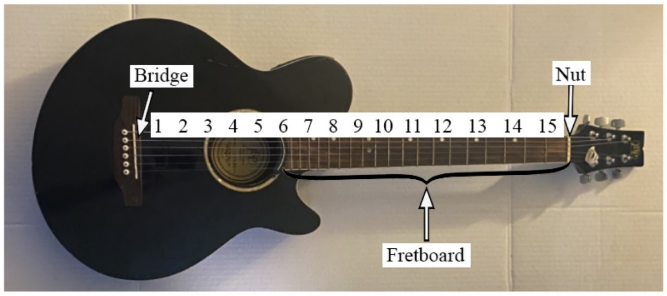


Figure 3: Guitar anatomy, including bridge, fretboard, and nut. The endpoints of the string are taken to be the bridge and the nut. The bridge is located on the body of the guitar, while the nut is located at the end of the fretboard near the tuning pegs. Picking/plucking locations are labeled 1-15 corresponding to Table 1.

Table 1: Locations of picking and plucking along the D string of an acoustic guitar measured in inches from the bridge.

| Position labels | Measurement from bridge (inches) |
|---|---|
| 1 | 1.5 |
| 2 | 3.125 |
| 3 | 4.6875 |
| 4 | 6.25 |
| 5 | 7.8125 |
| 6 | 9.375 |
| 7 | 10.9375 |
| 8 | 12.5 |
| 9 | 14.0625 |
| 10 | 15.625 |
| 11 | 17.1875 |
| 12 | 18.75 |
| 13 | 20.3125 |
| 14 | 21.875 |
| 15 | 23.4375 |

The sound produced by plucking the string at each of the 15 locations was recorded for roughly 8 seconds using the Audacity software and a Blue Snowball microphone. For a given location, a total of six recordings were made: three recordings were made using a plastic pick, and three recordings were made by plucking with a finger. This divided our data into two cases: plastic picking and finger plucking.

Each of these recordings was analyzed using MATLAB. An example of what the recordings look like after being read in MATLAB is displayed in Figure 4. Towards the beginning of the recording, the signal includes transient behavior generated from the striking of the string. Towards the end of the recording, the sound dissipates and the signal is less pronounced. Therefore, we performed all analysis on a sampled portion of the frequency where the data is more meaningful, specifically, from 20% to 40% of the total length of the recording. An example of such a sampling is shown in Figure 5.

## 3.2 Signal Processing

The audio file produced by each recording was analyzed using the Fast Fourier Transform (FFT). The Fourier transform takes as input a signal in the time domain and outputs a signal in the frequency domain [2, 3]. Peaks in a plot of the FFT output correspond to dominant frequencies present in the audio signal. The fundamental frequency of the D note is 147 Hz, and therefore, we expect a frequency of roughly 147 Hz to be most prominent in audio files. Subsequent peaks are to be expected at integer multiples of 147, corresponding to higher harmonics.

Figure 6 shows the single-sided amplitude spectrum obtained after applying the FFT

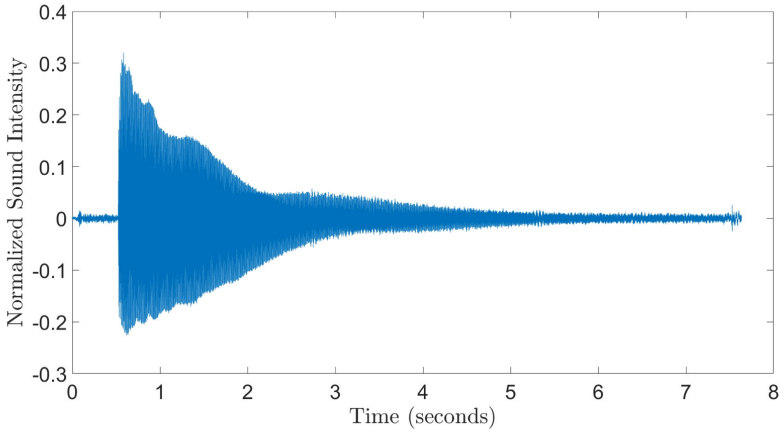


Figure 4: An example of the raw audio file produced by plucking the D string of an acoustic guitar at the location $\alpha = 6.25$in measured from the bridge.

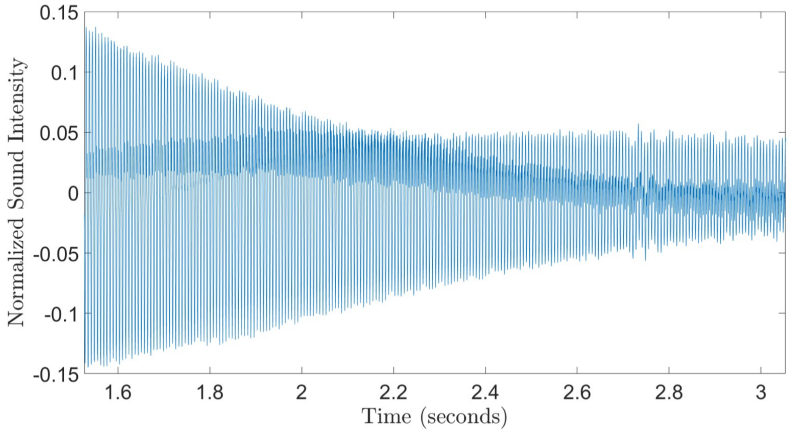


Figure 5: A sample portion of the frequency in Figure 4 from 20% to 40% of the total length of the recording.

to the signal shown in Figure 5. Moreover, we also set the minimum value for peaks to be 25 with a minimum distance of 100 between the peaks. This eliminated smaller peaks due to noise and made the prominent peaks more visible. Note that peaks occur at roughly 144.1 Hz, 294.7 Hz, 438.7 Hz, 586.8 Hz, 733.4 Hz, and 883.9 Hz. These values approximately correspond to the fundamental frequency for a D note and the frequencies of higher harmonics.

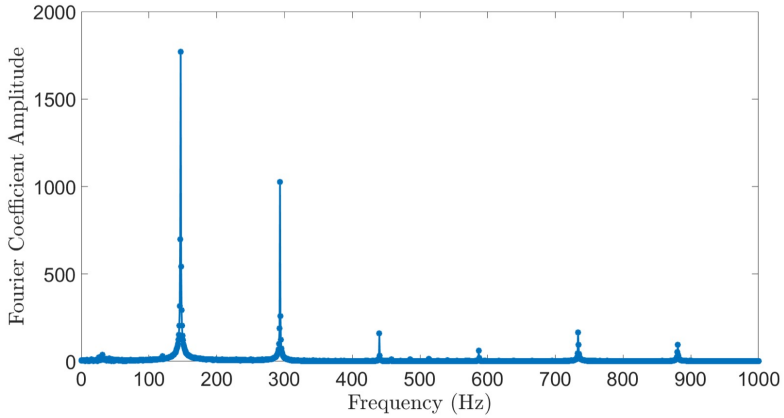


Figure 6: Single-sided amplitude spectrum obtained after applying the FFT to the audio signal in Figure 5. Here, $\alpha = 6.25$in measured from the bridge. After performing the FFT and setting the minimum peak height to 25 and minimum peak distance to 100, the magnitudes of the fundamental frequency and overtones are visible with peaks at roughly 144.1 Hz, 294.7 Hz, 438.7 Hz, 586.8 Hz, 733.4 Hz, and 883.9 Hz.

# 4 Results

We sought to compare the experimental values of $|a_{n,\alpha}|$ to those predicted by (9). However, note that (9) depends on the plucking height $\epsilon$. As we did not have a way to accurately measure the value of $\epsilon$ in our experiments, we instead studied the relative magnitude of $a_{n,\alpha}$ to $a_{1,\alpha}$. Specifically, we studied the ratio of the second, third, and fourth harmonics to the first one, which leads us to define the quantity

$$R_{n,\alpha} := \left| \frac{a_{n,\alpha}}{a_{1,\alpha}} \right|, \quad n = 2, 3, 4. \tag{10}$$

For each $n$ and each $\alpha$, let $R^t_{n,\alpha}$ denote the theoretical ratio prescribed by (10). For the theoretical values, (10) reduces to

$$R^t_{n,\alpha} = \left| \frac{\sin(n\pi\alpha/L)}{n^2 \sin(\pi\alpha/L)} \right|, \quad n = 2, 3, 4.$$

Note that this removes the dependence on the height $\epsilon$.

For each plucking location $\alpha$ and each harmonic $n$, we computed $R_{n,\alpha}$ using the first, second, third, and fourth harmonics obtained from the data collected after picking/plucking the string three times in the same location. We then averaged the resulting three ratios at each location to account for possible discrepancies in the picking/plucking mechanics. This process was carried out for the case of picking with a plastic pick and plucking with a finger. For fixed values of $\alpha$ and $n$, let $R^{(i)}_{n,\alpha}$ denote the ratio described by (10) for the $i$th recording. Here, the values $i = 1, 2, 3$ represent the three recordings made at each plucking location. Define $\bar{R}_{n,\alpha}$ to be the average ratio over the three recordings, i.e.,

$$\bar{R}_{n,\alpha} = \frac{1}{3} \sum_{i=1}^{3} R^{(i)}_{n,\alpha}.$$

In Figures 7 and 8, the values $\bar{R}_{n,\alpha}$ correspond to the heights of the experimental data points (orange), and the plucking locations $\alpha$ correspond to the values on the $x$-axis of each plot.

The first row of Figure 7 consists of the comparison between theoretical values and the data obtained using a plastic pick (referred to as "picked data"), while the second row consists the comparison between theoretical values and the data obtained by plucking with a finger (referred to as "plucked data"). We compare the relative magnitudes of the Fourier coefficients given by the theoretical prediction from (10) (blue) and those of the corresponding harmonics from the experimental data (orange).

Figure 8 includes the same data points as Figure 7 with the inclusion of error bars for the experimental results (black). For a given location $\alpha$, a given harmonic $n$, and a given instance of either plucking with a finger or with a plastic pick, the error bars in Figure 8 represent the quantity

$$\max_{i=1,2,3} \left| \bar{R}_{n,\alpha} - R^{(i)}_{n,\alpha} \right|$$

where $R^{(i)}_{n,\alpha}$ corresponds to $i$th recording. As with Figure 7, plots 8(a)-(c) correspond to data obtained using a plastic pick and comparisons between theoretical and experimental values for the second, third, and fourth harmonics, respectively. Plots 8(d)-(f) show similar plots for data obtained by plucking the string with a finger. Figure 7 highlights the qualitative trends in the data while Figure 8 gives a sense of the experimental error.

We quantify the difference between the theoretical and experimental values by using the $l^2$-norm. For a vector $\mathbf{v} = (v_1, v_2, \ldots, v_n)$, the $l^2$-norm, denoted $\| \cdot \|_2$, is defined by

$$\|\mathbf{v}\|_2 = \left( \sum_{i=1}^{n} v_i^2 \right)^{1/2}.$$

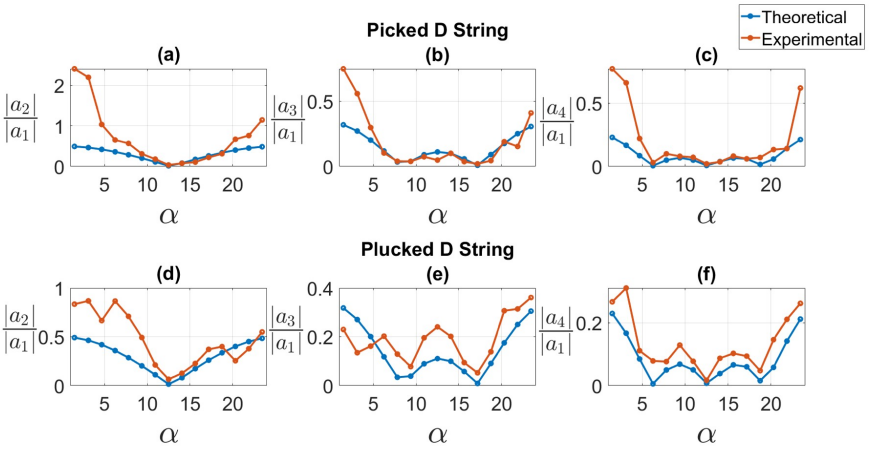


Figure 7: Plots (a), (b), and (c) display the comparisons between the theoretical model with the experimental data using the Fourier coefficients of the second, third, and fourth harmonics, respectively, for the D string data produced by using a plastic pick. Plots (d), (e), and (f) display the comparisons between the theoretical model with the experimental data using the Fourier coefficients of the second, third, and fourth harmonics, respectively, for the D string data produced by plucking with a finger.

For a fixed value of $n$, let $V_n$ denote the vector whose elements consist of the values $\bar{R}_{n,\alpha}$. Then $V_n$ consists of 15 elements corresponding to each of the plucking locations. In other words,

$$V_n = \left(\bar{R}_{n,1.5},\, \bar{R}_{n,3.125}, \ldots,\, \bar{R}_{n,23.4375}\right)$$

using the $\alpha$ values described in Table 1. Similarly, let $V_n^t$ denote the vector consisting of the 15 corresponding theoretical values $R_{n,\alpha}^t$ for a fixed value of $n$. For each plot in Figure 7, we computed

$$E_n = \left\| V_n - V_n^t \right\|_2 . \tag{11}$$

We refer to (11) as the $l^2$-error. These values are listed in Table 2.

In both the picked and plucked instances, the $l^2$-error is largest for the second harmonic ($n = 2$) when compared to the third ($n = 3$) and the fourth ($n = 4$) harmonics. The $l^2$-error for the plucked data generally decreases as $n$ increases, i.e., the error is smallest for $n = 4$ and greatest for $n = 2$. This pattern is not seen in the picked data as the $l^2$-error for $n = 4$ is greater than the $l^2$-error for $n = 3$. However, the overall improvement in agreement between experiment and theory when comparing $n = 2$ to higher values of $n$ may be due to the presence of nodes in the frequencies. In standing waves, such as guitar strings being strummed, a node is a location where there is no motion. In our case, the nodes occur where the magnitude of the ratio between the Fourier coefficients (10) is zero.

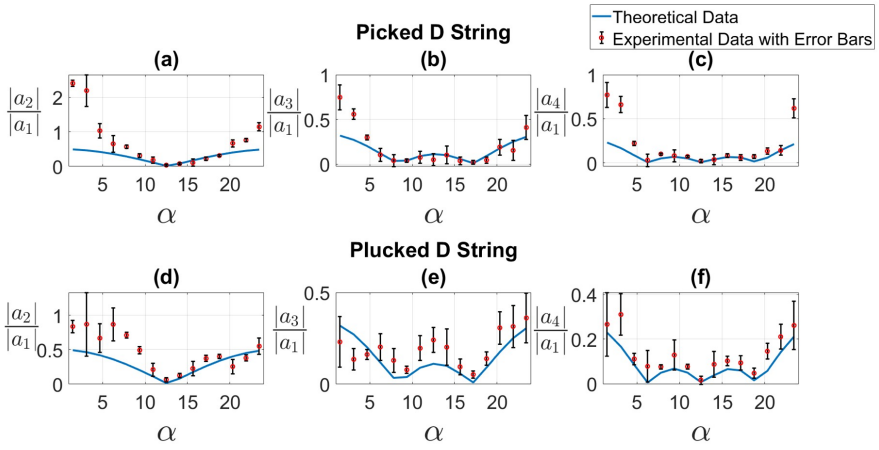


Figure 8: Plots (a), (b), and (c) display the error bars for the experimental data using the Fourier coefficients of the second, third, and fourth harmonics, respectively, for the D string data produced by using a plastic pick. Plots (d), (e), and (f) display the error bars for the experimental data using the Fourier coefficients of the second, third, and fourth harmonics, respectively, for the D string data produced by plucking with a finger.

In Figure 7, we see that the behavior near the nodes is qualitatively similar between the experiments and theory. Plots 7(a) and 7(d), show the value of $R_{2,\alpha}$ for each $\alpha$ for the picked and plucked data, respectively. In these two cases, we note that there is only one node. In plots 7(b) and 7(e) corresponding to $R_{3,\alpha}$, there are two nodes. In plots 7(c) and 7(f) corresponding to the values $R_{4,\alpha}$, there are three nodes. The increase in the number of nodes may act as a control on the error as these locations will result in more instances of very small Fourier coefficient amplitudes present in the data.

While discrepancies exist, the overall trend of each ratio $R_{n,\alpha}$ for $n = 2, 3, 4$ appears similar for both the experimental data and theoretical predictions in each subplot of Figures 7 and 8. Thus, the magnitude of the Fourier coefficients obtained in the experiments have qualitatively similar behavior as the prediction from the model.

# 5 Discussion

We explored comparisons between theoretical values for the magnitude of harmonics present in the wave equation to those obtained experimentally. While the behavior of the experiments and theory appear qualitatively similar, there were discrepancies in the quantitative values. The greatest errors appear to occur at picking/plucking locations near the endpoints of the string (Figures 7, 8). One reason for this may be that the

Table 2: The $l^2$-error $E_n$ given by (11) between the experimental values and the theoretical values for each subplot in Figure 7.

| Plot in Fig. 7 | Harmonic | $E_n$ |
|---|---|---|
| (a) | $n = 2$ | 2.7973 |
| (b) | $n = 3$ | 0.5498 |
| (c) | $n = 4$ | 0.8561 |
| (d) | $n = 2$ | 0.9632 |
| (e) | $n = 3$ | 0.3380 |
| (f) | $n = 4$ | 0.2327 |

piecewise linear description of a plucked string given by (3) as well as the one-dimensional wave equation used to model the string's motion given by (4) are too simplistic. In reality, a guitar string has a smoother initial profile than the one described by (3), and the endpoints of a guitar string are under tension from the bridge and nut causing bending of the string. This bending may be reason to introduce higher-order derivatives in the wave model, similar to those used to model beam deflection [4]. More sophisticated models that incorporate the deflection of the string and the contributions to the sound from the guitar's body may lead to more accurate results [4].

Discrepancies may also arise from experimental errors and limitations. One experimental limitation comes from outside noise that could not be controlled, such the string hitting the fretboard while vibrating. This may have led to noise in the recorded data and inaccuracies in the strength of the harmonics obtained. Another limitation was the inability to measure the height of the string that was plucked. We had to remove the dependence of the height by normalizing the data using the ratio between the Fourier coefficients of the $n$th and first harmonics. By improving the overall control in the experimental set-up, one may obtain more precise measurements and potentially more accurate results.

In addition to refining the theoretical model and experimental methods, one future direction would be to increase the number of recording locations in the hopes of obtaining a clearer picture of the relationship between the Fourier coefficients and plucking location. In addition, it would be interesting to apply the analysis presented here to different strings on the guitar, as each string has a different fundamental frequency and set of partials.

## Acknowledgments

We would like to thank the CSU Fullerton 2021 Summer Undergraduate Research Academy (SUReA) for providing funding to complete this project and the CSU Fullerton Mathematics Department for encouraging undergraduate research through the MATH 497/499 courses.

# References


[1] Boyce, W. E., & DiPrima, R. C. (2013). *Elementary differential equations and boundary value problems*. John Wiley & Sons, Inc.

[2] Brunton, S. L., & Kutz, J. N. (2020). *Data-Driven Science and Engineering: Machine Learning, Dynamical Systems and Control*. Cambridge University Press.

[3] Evans, L. C. (2010). Partial differential equations (Vol. 19). American Mathematical Society.

[4] Giordano, N., & Roberts, J. (2001, May). Musical acoustics and computational science. In *International Conference on Computational Science* (pp. 1041-1050). Springer, Berlin, Heidelberg.

[5] Hughes, J. R. (2000). Applications of Fourier Series in Classical Guitar Technique, *The College Mathematics Journal*, *31*(4), 300-303. https://doi.org/10.1080/07468342.2000.11974163

[6] Koss L. (2016). Differential equations in music and dance, *Journal of Mathematics and the Arts*, *10*(1-4), 53-64, http://dx.doi.org/10.1080/17513472.2016.1264050

## Authors


**Brandon Cugini**

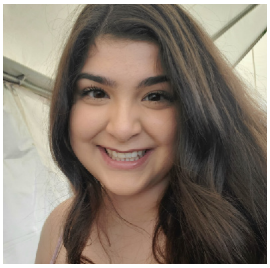

**Melissa Fernandez**

Melissa Fernandez is currently a Senior at Cal State Fullerton and is majoring in Biological Science, with a concentration in Ecology and Evolutionary Biology. She is a dedicated member of Dr. Shahrestani's Evolutionary and Genomics Research (EAGR) Lab, where she works with the rest of her team to establish Drosophila melanogaster as a model organism for the antibiotic resistance pathogen, Acinetobacter baumannii. She currently serves as this years' editor-in-chief for CSUF's Undergraduate Research Journal, dimensions. If not studying, her hobbies include gardening or binge-watching movies.

**Angelina Guzman**

Angelina's major is Biology with a concentration in ecology and evolutionary biology. In the future, she hopes to find a career working with a company to handle or help solve environmental and conservation issues. She would love to continue learning more about environmental restoration.

**Gabriela Guzman**

Gabriela Guzman is a recent graduate of California State University, Fullerton earning her bachelor's degree in biological science with a concentration in ecology and evolutionary biology. She plans to enroll in graduate school and continue her education in ecology. She hopes to pursue a career as a wildlife biologist while continuing to work with carnivores and rodents.

**Alisa Hernandez**

Alisa Hernandez is an undergraduate student majoring in biological science with a concentration in ecology and evolutionary biology and a minor in geography. She has been a research scholar in the Southern California Ecosystems Research Program (SCERP) since the summer of 2020, working with her advisor Dr. Bill Hoese on avian research. Following graduation in spring 2022, Alisa plans to continue pursuing her passions in conservation and ecological research in either the private or public sector.

**Michaelangelo Marcellana**

Michaelangelo Marcellana is a fourth-year undergraduate student at California State University, Fullerton, majoring in Biological Sciences with a concentration in Cellular and Developmental Biology. He plans to graduate in the Spring of 2023 and explore the medical field afterward. Overall, his goal is to attend medical school and pursue higher education to provide care for those in need.

**Vincent Mugica**

Vincent Mugica is a candidate for a B.S. in Geological Science at California State University, Fullerton. He is currently conducting a senior research thesis under the advisement of Dr. Valbone Memeti. In his research he interrogates the microgeochemistry of minerals in granitoids to illuminate processes occurring in magma plumbing systems in the crust. After he graduates, he intends on pursuing graduate studies in meteoritics.

**Ashleigh Quiroz**

Quiroz is a non-traditional student working on her Bachelor of Science in Geology at Cal State Fullerton. Her thesis focuses on the volcanology and petrology of Sierra Nevada, California and is overseen by Dr. Vali Memeti. After graduation, Quiroz has aspirations to seek higher education, though she is currently unable to narrow down one specific focus she would like to dedicate her studies towards.

**Leeza-Marie Rodriguez**

Leeza-Marie Rodriguez (she/her) recently received her Bachelor's degree in Biology from California State University, Fullerton, with a concentration in Marine Biology and minor in Chemistry in May 2022. At California State University, Fullerton, Leeza-marie conducted research investigating the effects of the non-indigenous spaghetti bryozoan, Amathia verticillata on the recruitment of the native Olympia oyster, Ostrea lurida. She will be attending the University of California, Santa Barbara in the fall to obtain her Ph.D.

**Victor Sanchez**

Victor Sanchez is a senior majoring in applied mathematics with a concentration in modeling and computation. Under the mentorship of Dr. Kristin Kurianski, Victor has worked on a research project where he explored classical guitar playing techniques through the use of signal processing. As a Sally Casanova Pre-Doctoral Scholar and an incoming research intern in MIT's Summer Research Program (MSRP), Victor hopes to continue to explore mathematical research and gain valuable experience that will help him along his journey in pursuing a Ph.D. in applied mathematics!

**Dahlia Serrato**

Dahlia Serrato is a fourth year biology major at California State University, Fullerton with a concentration in ecology and evolutionary biology. Through Project RAISE's Summer Research Experience program she assisted Dr. Kirby's geological analysis of sediment cores to explore the cause of wildfires. She plans to peruse research at CSUF further by a partnership with SCERP and environmental conservation at the federal level.


CSUF
TITANS
REACH
HIGHER